Normal-state transport and vortex dynamics in thin films of two structural polymorphs of superconducting NbN

K. Senapati, N. K. Pandey, Rupali Nagar, and R. C. Budhani*
Department of Physics, Indian Institute of Technology Kanpur, Kanpur-208016, India
(Received 10 April 2006; revised manuscript received 7 July 2006; published 29 September 2006)

The normal-state transport and the dynamic vortex response in simple cubic (sc) and face-centered cubic (fcc) polymorphs of NbN synthesized as epitaxial films of thickness $d_F \sim 2000$ Å using the technique of pulsed laser ablation are reported. The nonequilibrium sc phase of NbN stabilizes on (100) MgO at elevated deposition temperatures T_D (>200 °C), and over a restricted range of nitrogen pressure (p_{N_2}). The normal-state resistivity $\rho_N(T)$, critical temperature (T_c), critical current density [$J_c(T)$] and the temperature at which J_c goes to zero (T^*) depend largely on the extent of nonstoichiometry rather than the crystal symmetry of these films. The divergence of $\rho_N(T)$ on cooling before the onset of T_c is analyzed in the framework of a grain boundary model in which electron transmittivity Γ across the grains is considered explicitly. The zero-field J_c deduced from screening measurements follows a temperature dependence of the type $J_c(T) \sim (1-T/T_c)^{\beta}$, with β increasing from 0.75 to 1.2 as the $d\rho_N(T)/dT$ changes sign from negative to positive. The films with negative $d\rho_N(T)/dT$ are disordered and possibly nonstoichiometric. For stoichiometric films, the temperature dependence of J_c in the mixed state and the variation of the critical temperature T^* as a function of applied dc field are consistent with the model of thermally activated flux creep.

DOI: 10.1103/PhysRevB.74.104514 PACS number(s): 74.25.Qt, 74.81.Bd

I. INTRODUCTION

Superconductivity in thin films of NbN has been widely studied[1–12] in the past decades with the motivation to use them for Josephson junction based device applications because of their relatively high transition temperature T_c ($\sim$16 K). However, the large magnetic penetration depth ($\lambda \sim 250$ nm) and the small coherence length ($\xi < 5$ nm) of polycrystalline NbN films pose major limitation for such applications. Therefore, many studies on NbN have focused on preparation and improvisation of single crystal thin films.[8–12] From the viewpoint of basic physics, the degree of structural imperfections and its repercussions on superconductivity are interesting issues to address. For example, a gapless behavior in NbN films has been demonstrated by Lamura *et al.*,[13] depending on the degree of granularity. Multilayers of NbN with other metal nitrides such as GdN,[14] TaN,[15] and AlN (Ref. 16) have also been synthesized to study the fundamental aspects of proximity effect, Josephson coupling and vortex dynamics.

Recently, Treece *et al.*[11] have demonstrated that NbN films grown on MgO (100) using pulsed laser deposition (PLD) acquire a metastable primitive cubic structure (space group $Pm3m$) when deposited at substrate temperature in the range of 400 to 700 °C. The usual rocksalt structure (space group $Fm3m$) stabilizes only below this temperature window. Interestingly however, this simple cubic phase has not been observed in sputter-deposited films.[17,18] Electronic band structure calculations for this new phase also shows that it is energetically unfavorable[19,20] compared to the fcc rocksalt structure of NbN.

In this paper we report confirmation of the observation of Treece *et al.*[11] The simple cubic phase is formed in a restricted window of pulsed laser deposition conditions. Outside this window, the well known fcc structure of NbN is stabilized. We have undertaken a systematic study of the mixed state dynamics and the normal-state transport behavior of these two structural polymorphs of NbN and discussed how granularity affects the transport and screening properties of such thin films. We observe that the formation of stoichiometric NbN depends critically on the N_2 pressure during deposition. Our measurements have demarcated a well-defined window of temperature and N_2 pressure (p_{N_2}) for controlled growth of the simple cubic and fcc structures of NbN. Higher deposition temperatures favor formation of metallic films showing positive, albeit small, temperature coefficient of resistance (TCR), where as those deposited at lower temperatures with nonoptimal p_{N_2} have diverging resistivity on cooling before the onset of superconductivity. However, the normal-state transport as well as the dynamic vortex response indicate a higher transparency of grain boundaries in these films. In addition, we find that the exact crystal symmetry of the films does not affect the dynamics of the superconducting state.

II. EXPERIMENTAL

Thin films of NbN were prepared on single crystal (100) MgO substrates by pulsed laser ablation of a high purity Nb target in a controlled ultra high purity (99.9996) N_2 environment. A KrF excimer laser (248 nm) operated at 20 Hz was used for ablation with pulse energy density of ~ 5 J/cm^2 on the surface of the target. The pressure of N_2 during the film growth has been used as a means of controlling the overall fraction of pure NbN in the films. A series of films with thickness $\sim$2000 Å was prepared in this way at 200 °C at several setting of the N_2 pressure (p_{N_2}). In order to see the effects of deposition temperature (T_D) on structure and properties, we have also deposited films of similar thickness at 400, 500, and 600 °C. The standard θ-2θ x-ray diffraction has been utilized to verify the structure of these films and

scanning electron microscopy (SEM) has been used to characterize their surface topography. The superconducting transition temperature and the normal-state resistivity of the films were measured using the standard four terminal method, while the dynamics of vortices in the superconducting state was investigated with a miniature Hall-sensor based ac susceptometer.[21] In this apparatus, the response of a superconducting film to an ac excitation is picked up by a small Hall sensor, placed close to the surface of the film. The in-phase and quadrature components of the measured Hall-signal are then decomposed by use of a lock-in amplifier. Following a model by Gilchrist and Konczykowski,[22] the real and imaginary parts of the ac susceptibility are calculated from the relations $\chi' = T'_H - 1$ and $\chi'' = T''_H$ respectively. Here T'_H and T''_H are the real and imaginary parts of complex transmittivity defined as

$$T'_H = \frac{[V'(T) - V'(T \ll T_c)]}{[V'(T \gg T_c) - V'(T \ll T_c)]} \quad (1)$$

$$T''_H = \frac{[-V''(T)]}{[V'(T \gg T_c) - V'(T \ll T_c)]} \quad (2)$$

where, V' and V'' are the in-phase and quadrature components of the Hall-probe voltage measured at the fundamental frequency. The third harmonic susceptibility can also be obtained by measuring the Hall-probe voltage (V_{3f}) at triple the frequency of excitation using the relation

$$|T_{H3}| = \frac{|V_{3f}(T)|}{[V'(T \gg T_c) - V'(T \ll T_c)]}. \quad (3)$$

III. RESULTS AND DISCUSSION

A. Structural characterization

The θ-2θ x-ray diffraction measurements revealed a highly (h00) oriented growth along the (100) axis of the substrate. Figure 1 compares the x-ray diffraction patterns of NbN films deposited at 200, 300, 500, and 600 °C in 80 mTorr of nitrogen. Clearly, the films deposited at temperatures above 200 °C show all (h00) reflections indicating a simple cubic structure in agreement with the results of Treece *et al.*[11] On the other hand, the (h00) reflections of odd h, which have vanishing atomic structure factors for an fcc lattice are missing in the film deposited at 200 °C. The average grain size of the films was calculated from the full width at half maximum (FWHM) of the high-angle Bragg peaks [(200) and (400)], using the Debye-Scheerer formula[23]

$$D = \frac{0.97\lambda}{\beta \cos\theta}, \quad (4)$$

where λ and β are the x-ray wavelength and FWHM of the peak, respectively. We find a monotonic increase in the grain-size from ~210 to ~290 Å as the deposition temperature is varied from 200 to 600 °C. The larger grain size of the films deposited at the higher temperature is a consequence of the availability of higher crystallization energy during film growth. In addition to the increase in the grain size, a gradual shift of the lattice parameter towards the bulk value is also observed as a function of increasing deposition temperature. Figure 2 shows a comparison of the x-ray diffraction patterns of films deposited at 600 °C at varied nitrogen pressures. Surprisingly, the simple-cubic phase [evident from the (100) peak] is observed only in the films deposited at the optimal nitrogen pressure (80 mTorr). However, SEM micrographs of the films showed a smooth surface topography without any notable difference between the two phases of NbN.

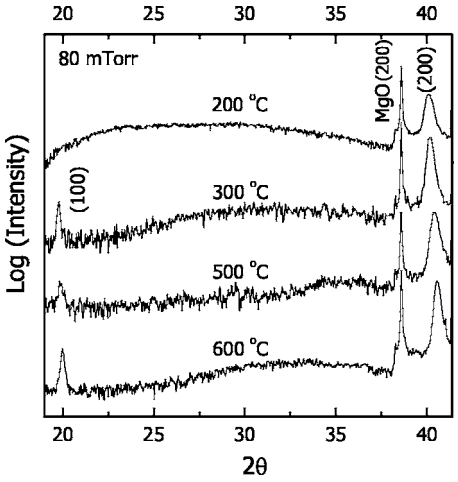

FIG. 1. $\theta-2\theta$ x-ray diffraction pattern of NbN films deposited at 200, 300, 500, and 600 °C on (100) MgO substrate at nitrogen pressure of 80 mTorr. The typical growth rate of NbN films was ~4 Å/s.

It should be noted here that fabrication of good quality films from elemental metal targets is quite nontrivial with pulsed laser ablation. This technique relies on the formation of a local superheated region on the target, which then ex-

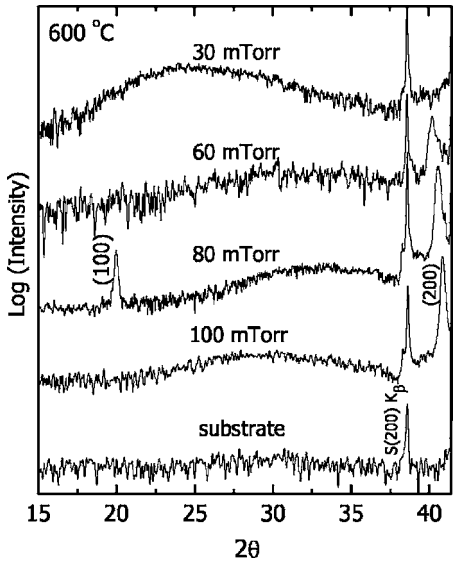

FIG. 2. $\theta-2\theta$ x-ray diffraction pattern of NbN films deposited at 30, 60, 80, and 100 mTorr of N_2 pressure and 600 °C substrate temperature. Diffraction peaks due to the substrate and fcc and simple cubic structures are marked in the figure.

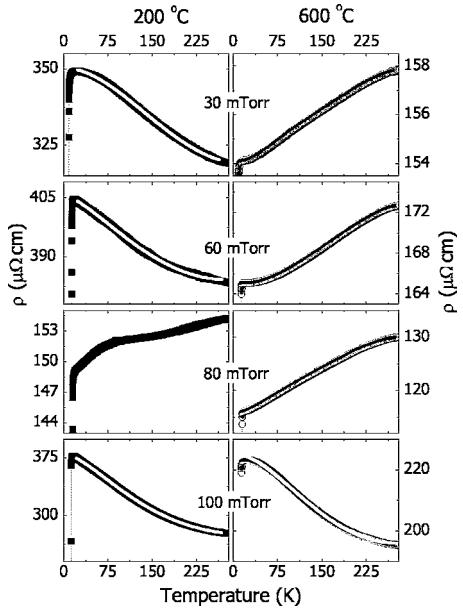

FIG. 3. The temperature dependence of the normal-state resistivity of the NbN films deposited at 200 °C (left hand side panels) and 600 °C (right hand side panels). The solid lines are fits to the grain-boundary model (see text for details).

plodes as a plasmonic plume maintaining the stoichiometry of the target.[24] The high thermal conductivity of elemental metals, however, hinders the formation of a superheated spot on the target and the material is removed by splashing, rather than ablation. Therefore, parameters such as laser energy density, pulse repetition rate, and target-to-substrate distance need to be optimized very carefully. In view of such limitations, the smooth surface and the highly oriented crystalline structure of our NbN films is encouraging.

B. Electrical transport

The temperature dependence of the electrical resistivity $[\rho_N(T)]$ of the NbN films deposited at 200 and 600 °C under different conditions of N_2 pressure is shown in Fig. 3. In most of the films, a negative temperature coefficient of resistivity (TCR) is observed when their room temperature resistivity is higher than ≈170 $\mu\Omega$-cm. But the TCR is positive for the low resistivity films. This correlation[25] between the sign of TCR and room temperature resistivity indicates a disorder dominated electron transport in these films. While in homogeneously disordered alloys such as amorphous films of MoGe (Ref. 26) or AuGe,[27] weak localization plays a dominant role in the temperature dependence of resistivity,[28] in the present case of well-crystallized films grain boundary scattering should dominate the transport. We have examined our data using the grain boundary model proposed by Reiss *et al.*,[29] which can be viewed as a quantum correction to the classical Drude conductivity. The model[29] attributes the reduced conductivity of the granular media to the number density and quantum transparency of grain boundaries crossed by an electron during two successive scattering events. The effective mean free path is expressed as

$$L_{\text{eff}} = L\Gamma^{L/D}, \tag{5}$$

where L is the mean free path in the absence of granularity, Γ the transmission probability of electrons through the grain boundary, and D is the mean grain size. The conductivity is thus written as

$$\sigma(T) = \left(\frac{ne^2}{mv_F}\right) L\Gamma^{L/D}, \tag{6}$$

where m, v_F, and n are the mass, Fermi velocity, and density of conduction electrons, respectively. This model has also been employed by Tyan *et al.*[7] and Nigro *et al.*[30] to analyze the normal-state transport behavior of reactive dc and reactive magnetron sputtered NbN films respectively. The values of Γ obtained in these two cases, however, differ considerably ($\sim 10^{-1}$ from Tyan *et al.*[7] and 10^{-5} from Nigro *et al.*[30]). We have fitted our data in Fig. 3 to Eq. (6) assuming Γ and n as temperature independent parameters. The fittings are shown as solid lines in the figure. The only term that contributes to temperature dependence of resistivity in Eq. (6) is the mean free path given as $\frac{1}{L(T)} = \frac{1}{l_e} + \frac{1}{l_{\text{in}}(T)}$, where l_e is the elastic mean free path and $l_{\text{in}}(T)$ the inelastic mean free path whose temperature dependence is expressed as $l_{\text{in}}^{-1}(T) \approx \alpha T^p$. The exponent p is close to 2 and α is a proportionality constant. We obtain excellent fits to our data for the films with negative TCR for values of Γ close to 0.15 with a sample-to-sample spread of ~0.015, which can be accommodated into the error scale. The mean grain size (21 and 29 nm for the films deposited at 200 and 600 °C, respectively) was taken from the x-ray diffraction measurements of respective films while fitting to Eq. (6). The average electron density for the best fits comes out to be of the order of 10^{27} /m^3 using a Fermi velocity of 0.9×10^6 m/s from the literature.[31] The metallic samples follow an almost linear temperature dependence over a wide range of temperature. This is in accordance with the Bloch-Gruneisen formula[32] for phonon-scattering-limited conductivity.

In order to address the influence of granularity on critical temperature we show in Fig. 4 the temperature dependence of electrical resistivity $[\rho(T)]$ in the temperature range 4.2 to 18 K of a series of films deposited at 200 °C. The resistivity of all films is characterized by a sharp transition to the superconducting state at $T < 16$ K. In all cases the transition width ΔT_c, defined as the temperature over which $[\rho(T)]$ changes from 90 to 10 % of the extrapolated normal-state value is below 1 K. The figure reveals a marked effect of the N_2 pressure (p_{N_2}) on the transition temperature. The inset of Fig. 4 shows the T_c as a function of p_{N_2} normalized to the T_c of the film deposited at $p_{N_2} = 80$ mTorr. We observe a well defined peak in the T_c vs p_{N_2} graph for the films deposited at 200 and 600 °C in the vicinity of ~80 mTorr. This result suggests that the optimum stoichiometric fraction of NbN in these films is independent of the deposition temperature. A similar non-monotonic dependence of T_c on N_2 pressure has been reported by Bacon *et al.*[3] for sputter-deposited films. Here it is important to point out that while a large reduction in T_c along with a negative TCR in the normal state is seen in films deposited at lower p_{N_2}, the transi-

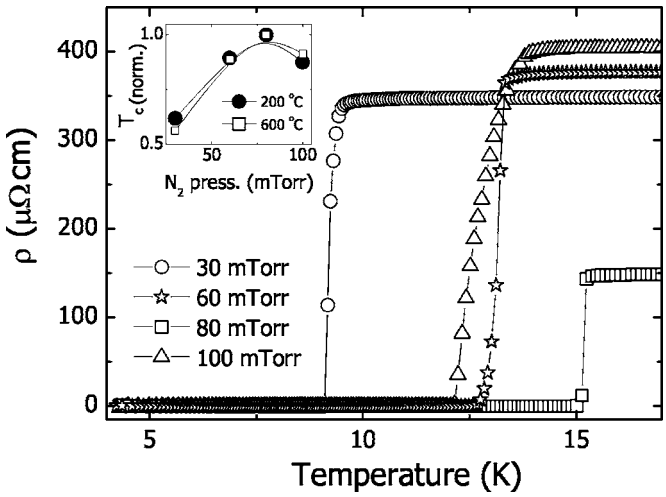

FIG. 4. Electrical resistivity of the NbN films in the superconducting transition region. The inset is a plot of $T_{c(\text{onset})}$ as a function of the N_2 pressure for films deposited at 200 and 600 °C on (100) MgO.

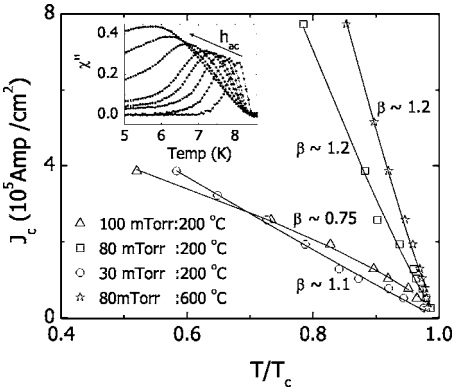

FIG. 5. The zero dc-field critical current density J_c calculated from the imaginary part of complex ac susceptibility (χ'') is plotted against the normalized temperature T/T_c. The solid lines are fits to the equation $J_c \sim (1-T/T_c)^{\beta}$. Inset shows the χ'' for a NbN films deposited at 200 °C and 30 mTorr N_2 pressure. Measurements were performed at 121 Hz with varying magnitude of the ac field in the range of 0.5 to 15 Oe.

tion width remains narrow in all cases. This is unlike the behavior of the resistive transition in heavily granular NbN-BN cermet films.[33]

Superconductivity in polycrystalline NbN films is often modeled as arrays of Josephson junctions.[5,6,13,29,30,34] In an ideal granular SC, with junction resistances above the quantum pair resistance ($h/2e^2 \sim 6$ kΩ), the transition temperature is decided by the degree of phase fluctuation in the intergranular region and quasiparticle tunneling effects.[35] The stoichiometric NbN films with critical current close to depairing current, however, cannot be classified as granular. Similarly, in nitrogen deficient films (NbN_{1-x}), the low resistive intergranular matrix inhibits a Josephson coupling picture. In fact, the intergranular disordered NbN matrix might also be superconducting with a lower T_c than the T_c of the stoichiometric NbN. Thus a proximity coupled *S-N-S* picture appears more appealing for such films. The initial rise in T_c as a function of N_2 pressure (in the inset of Fig. 4) also suggests an increase in the density of stoichiometric NbN grains. Further increase in N_2 pressure above the optimum value reduces the coupling between NbN grains due to accommodation of extra nitrogen atoms in the disordered intergranular regions. In this case the physics of a true granular superconductor such as Al_xO_{1-x} might be applicable.[36]

C. Vortex dynamics

1. Screening critical current density

The imaginary component (χ'') of the fundamental ac susceptibility (χ) measured at a fixed ac field of frequency 121 Hz, for a film deposited at 200 °C and 30 mTorr N_2 pressure is shown as a function of temperature in the inset of Fig. 5. These data were taken at several values of the ac field ranging from 0.5 to 15 Oe. We have calculated the screening critical current density of the films following the method of Clem and Sanchez[37] who have shown that for a superconducting disc of radius R and thickness d, placed under a transverse ac excitation of the form $h=h_0 \exp(-i\omega t)$, the real and imaginary components of complex fundamental ac susceptibility are given as[34]

$$\chi' = \frac{2\chi_0}{\pi}\int_0^{\pi}(1-\cos\theta)S[(x/2)(1-\cos\theta)]\cos\theta d\theta \quad (7)$$

and

$$\chi'' = \frac{2\chi_0}{\pi}\int_0^{\pi}\{-S(x)+(1-\cos\theta)S[(x/2)(1-\cos\theta)]\}\sin\theta d\theta, \quad (8)$$

where $x=h_0/H_d$, $H_d=J_c d/2$, and $\chi_0=8R/3\pi d$. This expression, however, assumes a critical current density (J_c) independent of the applied ac field. The function S is defined as

$$S(x) = \frac{1}{2x}\left(\cos^{-1}\left[\frac{1}{\cosh x}\right] + \frac{\sinh x}{\cosh^2 x}\right). \quad (9)$$

In the limit of small ac field, the above expressions for χ' and χ'' approximate to

$$\chi' = -\chi_0\left(1-\frac{15}{32}x^2\right) \quad (10)$$

and

$$\chi'' = \chi_0 x^2/\pi. \quad (11)$$

Numerical calculations by Clem and Sanchez[37] shows that the peak in χ'' appears at $x=1.942$, which leads to the relation $J_c=h_0/1.942d$. The critical current density calculated in this way for NbN films deposited at 200 °C under various p_{N_2} is shown in the main panel of Fig. 5. This figure also shows the J_c of the film deposited at 600 °C under optimal p_{N_2} (80 mTorr). Here we recall that the crystal symmetry of these films is simple cubic unlike of those deposited at 200 °C, which are fcc. The magnitude and temperature dependence of J_c appears to be independent of the exact crystal

symmetry for the films prepared under optimal p_{N_2}. However, on both sides of the optimal p_{N_2}, a drastic drop in J_c is evident in Fig. 5. We also notice a slight convex curvature in J_c vs T/T_c plot of the film deposited at higher (100 mTorr) N_2 pressure. This tendency of J_c to reach saturation at the higher T/T_c can be attributed to excess nitrogen in the films, which may reduce the overall condensate density.

The results of this contactless method of measuring J_c agree with transport J_c in homogenous films of low and high-T_c materials.[38,39] Since the magnetic penetration depth λ in the present case is smaller than the film thickness, the induced screening currents are also uniform and maximum sustainable by the superconducting state. In inhomogeneous systems, however, a screening measurement yields intragranular currents in addition to some amount of grain averaged current, which is sustained by the Josephson or proximity coupling between adjacent grains. The Josephson coupled current has a profound effect on the overall magnetic susceptibility of the material. Most notably, the weak superconducting order parameter in the intergranular material has a distinctly lower critical current density as compared to the intra-granular J_c. The existence of two characteristic critical currents manifests as two distinct peaks in the imaginary component of the fundamental ac susceptibility. However, unlike typical polycrystalline and granular superconductors,[39,40] we find only one peak in the temperature dependence of χ'' of our NbN films (shown in the inset of Fig. 5). This observation suggests that the SC-order parameter remains robust in the grain boundaries of these films. This inference is also consistent with the large transmission probability Γ for carrier transport across grain boundaries in the normal state as discussed earlier. The exact temperature dependence of J_c in a granular superconductor depends upon parameters including grain-size, coupling between grains, flux creep, and depinning effects.[41] To apprehend this fact, we have fitted the temperature dependence of J_c to a relation of the type $J_c \sim (1-T/T_c)^{\beta}$, where β is used as a fitting parameter. The fitted curves are shown as solid lines in Fig. 5 along with the values of β extracted from the fits. For a pure Ginzburg-Landau (GL) behavior of the critical current, one expects $\beta \sim 1.5$.[41] We find that maximum deviation in β from the ideal GL value occurs in the film deposited at the 100 mTorr N_2 pressure.

Kampwirth *et al.*[2] have modeled thick NbN films with columnar texture as an ordered array of Josephson-coupled grains with identical intergranular regions. The critical current density (J_c) of such a system is given by the Ambegaokar-Baratoff[42] (AB) expression for the Josephson current in a *S-I-S* junction, which yields a monotonic temperature dependence of the type $J_c \sim (1-T/T_c)$ close to the critical temperature T_c. While this model does not apply to our stoichiometric NbN films where J_c is close to the depairing current, it may be valid for nonoptimal p_{N_2} films, particularly those deposited at 100 mTorr p_{N_2} and show a highly suppressed J_c with $\beta \simeq 0.75$.

In Fig. 6 we compare the temperature dependence of the in-field J_c of the simple cubic ("panel A") and fcc ("panel B") NbN films deposited under optimal N_2 pressure (80 mTorr). The solid lines are fittings to the relation J_c

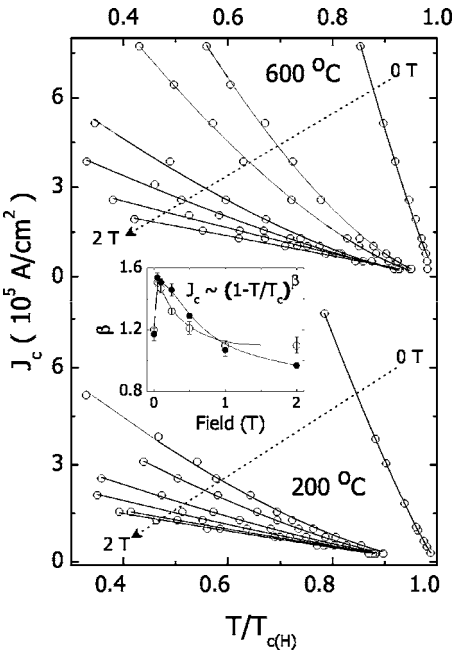

FIG. 6. Critical current density of NbN films deposited at 200 and 600 °C at 80 mTorr N_2 pressure in the presence of dc fields of 0.05, 0.1, 0.25, 0.5, 1.0, and 2.0 T perpendicular to the plane of the sample. Solid lines are the fits of the form $(1-T/T_{c(H)})^{\beta}$. The values of β [(○) 200 °C and (●) 600 °C] extracted from these fittings are plotted as a function of dc field in the inset.

$\sim (1-T/T_{c(H)})^{\beta}$, where $T_{c(H)}$ is the onset temperature of χ'' in presence of a dc field H. While the critical current drops significantly in both types of samples on the application of a small (~500 Oe) dc field, the suppression of J_c is sharper in the case of the fcc structure. At first instant, this difference points towards the crystal symmetry. However, one has to take into account the larger grain size of the simple cubic film due to the higher deposition temperature (600 °C) used in this case and the field-induced suppression of superconductivity in the intergranular material if the grain boundaries are diffused, which is likely to be the case due to the lower adatom mobility in films deposited at 200 °C. The average grain size of the sc film is ~290 Å while it is only ~210 Å for the fcc film. Since the current carrying capacity of a single grain (intragranular J_c) is determined by the total condensation energy of the grain, the magnitude of intragranular J_c is expected to scale with the crystallite size. It is also likely that clean grainboundaries of 600 °C films give rise to strong flux pinning as in the case in Nb_3Sn.[43] In addition to the suppression of J_c, we also notice a drastic change in its temperature dependence at low dc fields. The low field J_c goes as $\sim (1-T/T_{c(H)})^{1.5}$ as seen in the inset of Fig. 6. At still higher fields β tends to unity. The temperature and magnetic field dependence of J_c in the mixed state of a type-II superconductor is decided by the depinning mechanism of flux lines. In the thermally activated flux creep scenario of dissipation, the electric field generated due to flux motion is given as;[43]

$$E = 2\Omega d \exp\left(\frac{-U_0}{k_\beta T}\right)\sinh\left(\frac{BJVa}{k_\beta T}\right), \tag{12}$$

where B is the magnetic induction; V, the volume of the flux bundle over which the Lorentz force acts; U_0, the pinning potential; a, the width of the pinning potential well; Ω, the attempt frequency of hopping process; and d, the hopping distance. Defining E_c as the minimum electric field chosen for the measurement of critical current, we have

$$J_c(T,B) = \frac{k_\beta T}{BVa}\sinh^{-1}\left[\left(\frac{E_c}{2d\Omega}\right)\exp\left(\frac{U_0(T)}{k_B T}\right)\right]. \tag{13}$$

Linearization of the sinh function yields

$$J_c(T,B) = \frac{U_0(T)}{B}. \tag{14}$$

For a given B, the temperature dependence of J_c comes from $U_0(T)$ under the assumption that the activation volume V is temperature independent. In a single vortex pinning picture, one can write $U_0(T)$ as $\sim H_c^2(T)\xi^n(T)$, which with GL temperature dependence of $H_c(T)$ and $\xi(T)$ yields

$$U_0(T) \sim (1-t)^2(1-t)^{-n/2} = (1-t)^{2-n/2}. \tag{15}$$

Here $n=0$, 1, 2, or 3 depending on the relevant length scale for the energy of the flux line. For grain boundary pinning in very thin films (thickness $\approx\xi$) at low flux densities (FLL spacing $\gg$ grain size), the pinning volume is linear in ξ. Under this approximation we see that $U_0(T)\sim(1-t)^{3/2}$, which is consistent with the behavior of J_c at low fields. As the FLL spacing $[a_0=1.075(\phi_0/B)^{1/2}]$ becomes smaller with the increasing field, flux lines will be accommodated within the grains, for these, $U_0(T)\sim H_c^2(T)\xi^2(T)$. This yields a temperature dependence of the type $U_0(T)\sim(1-t)$. This conclusion is consistent with the data taken at 2 T for which $a_0 \simeq 34$ Å.

2. Third harmonic susceptibility

The onset of a nonlinear response to the driving ac field in the mixed state of a superconductor is characterized by the appearance of third harmonic susceptibility (χ^{3f}) while cooling below T_c. We have measured the third harmonic ac susceptibility of the NbN films in the presence of a dc-field collinear with the ac field of frequency $\sim$121 Hz along the film normal. The third harmonic signal of a NbN film deposited at 200 °C and 80 mTorr p_{N_2} is shown in the inset of Fig. 7. The onset of χ^{3f} marks the temperature T^* below which the superconductor is able to sustain a dissipationless current. Since the flow of such a current in the mixed state is decided by pinning of flux lines, one can argue that T^* is the depinning temperature (T_{dp}). The literature on high-T_c cuprates, however, identifies T^* with the irreversibility temperature T_{irr} above which dc magnetization becomes reversible.[38,44] The identification of T_{dp} with T_{irr} has been debated considerably in the recent literature.[45–48] There are materials, particularly low T_c alloys, which show a nonzero critical current in the temperature regime where the magnetization is fully reversible.[48] The main panel of Fig. 7 shows

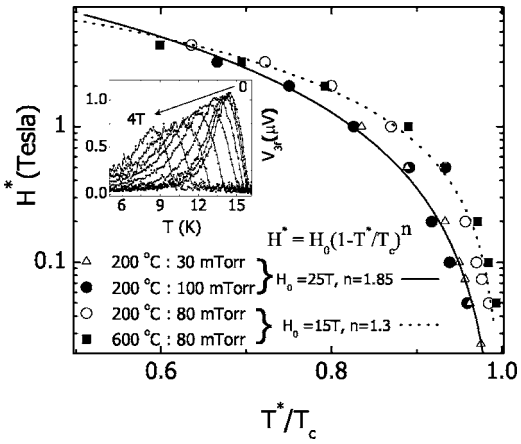

FIG. 7. The critical field H^* of NbN films as a function of the normalized temperature T^*/T_c. The solid and the dotted lines are the calculated curves using the relation $H^*\sim H_0(1-T^*/T_c)^n$. Inset shows the third harmonic signals of 200 °C, 80 mTorr film, as captured by the Hall-probe susceptometer. Curves are shown for measurements at dc fields in the range of 0 to 4 T.

the T^* lines of our NbN films on the H-T plane deduced from the onset temperature of the χ^{3f}. Since the frequency of measurement of χ^{3f} is small, we consider the data of Fig. 7 as the zero-frequency limit of T^*. We note that the critical temperature T^* of the fcc phase well as the sc phase films deposited under the same p_{N_2} (shown as ○ and ■ respectively, in Fig. 7) is identical within the accuracy of these measurements. The $H^*(T)$ is found to follow a relation of the type $H^*(T) = H_0(1-T^*/T_c)^n$ with $H_0=15$ T and $n=1.3$ (shown as the dotted line in Fig. 7). However, the exponent n is markedly different for the films deposited at N_2 pressures away from the optimum value. For these films, the fitting as shown in Fig. 7 (solid line), yields $n\approx1.85$ and $H_0\approx25$ T. The temperature dependence of H^* in $YBa_2Cu_3O_7$ has been deduced in the framework of thermally activated depinning of flux lines by Yeshuran and Malozemoff,[45] assuming that the activation energy for depinning scales as $U_0(T)\sim H_c^2(T)a_0^2\xi(T)$. Here it has been assumed that the extent of the pinning volume orthogonal to the field direction is independent of $\xi(T)$ in the high field limit $[a_0<\xi(T)]$. Our analysis of the $J_c(T)$ data of Fig. 6 suggests that for stoichiometric NbN films the power n in $H^*\sim(1-T^*/T_c)^n$ should vary between 1.5 and 1 as the flux density increases in the system. The average value of $n=1.3$ extracted from the fit over a wide temperature range ($T/T_c\approx0.6$ to 1) is consistent with the depinning picture. In the case of the nonoptimal p_{N_2} films, the presence of large scale inhomogeneities makes understanding of the temperature dependence of H^* rather difficult. It also needs to be emphasized here that in low T_c alloys the separation between the irreversibility line and $H_{c2}(T)$ line in the H-T phase space is so small[46–48] that it may well be within in the accuracy of our measurement. In that event, the data shown in Fig. 7 essentially reflect the behavior of the $H_{c2}(T)$. Figure 7 reveals that H_0 is considerably smaller ($\sim$15 T) for the films with the higher T_c as compared to the $H_0\approx25$ T for the low T_c films. Although H_0 is by no means equivalent to $H_{c2}(0)$, it differs only by a multiplication factor. Hence, the low T_c

films with less conducting grain boundaries (smaller effective mean free path) have higher $H_{c2}(0)$ as compared to the $H_{c2}(0)$ of films with more conducting grain boundaries. This result follows from the Ginzburg-Landau-Abrikosov-Gorkov theory for H_{c2} of disordered superconductors. The theory predicts a higher H_{c2} in samples with reduced electron mean free path as a result of the suppression of Pauli paramagentic effect, which limits the H_{c2}.[49] Such effects are seen abundantly in disordered low T_c alloys such as Nb_3Sn, for example.[50]

IV. CONCLUSIONS

We have carried out a detailed study of the possible manifestations of inhomogeneities and crystal symmetry in the normal-state transport as well as in the vortex dynamics of PLD grown NbN films, which have been stabilized in both fcc and sc structures by precise control of the PLD growth parameters such as temperature and N_2 pressure. The x-ray diffraction measurements indicate a well-oriented growth along the (100) direction with average grain size varying from $\sim$210 to $\sim$290 Å as the T_D is increased from 200 to 600 °C. The normal-state transport as well as the dynamical behavior of flux lines in the SC state indicate that the intergranular matrix is highly transparent to the normal as well as superconducting carriers in these films, unlike in the Josephson coupled *S-I-S* granular films. The superconducting transition temperature was found to be strongly dependent on the nitrogen stoichiometry of the films. Under optimal deposition conditions, the T_c and J_c as high as 16 K and $7\times10^5/\mathrm{cm}^2$ at 12 K were obtained. The temperature dependence of the J_c extracted from the ac-susceptibility data in zero dc field and also in the presence of a dc field for the films deposited under optimal p_{N_2} have been analyzed in the framework of thermally activated flux creep. While we see two distinct phases of NbN, and the energetically less stable simple cubic phase is perhaps stabilized because of the high kinetic energy of the ablated atoms in PLD, no distinctive feature of crystal symmetry are seen in the superconducting properties. This result is somewhat surprising in view of the fact that the density of states calculations for the simple cubic phase yield a much larger DOS at the E_F.[20] It is quite possible that extrinsic effects such as granularity mask the differences, or perhaps, the observed structure has a different symmetry from the stoichiometric *Pm3m*, for which electronic calculations are available.

ACKNOWLEDGMENTS

This research has been supported by a grant from the Department of Science and Technology, Government of India.

*Electronic address: rcb@iitk.ac.in

[1] S. Wolf and W. H. Lowrey, Phys. Rev. Lett. **39**, 1038 (1977).
[2] R. T. Kampwirth and K. E. Gray, IEEE Trans. Magn. **17**, 565 (1981).
[3] D. D. Bacon, A. T. English, S. Nakahara, F. G. Peters, H. Schreiber, W. R. Sinclair, and R. B. van Dover, J. Appl. Phys. **54**, 6509 (1983).
[4] S. Thakoor, J. L. Lamb, A. P. Thakoor, and S. K. Khanna, J. Appl. Phys. **58**, 4643 (1985).
[5] K. E. Gray, R. T. Kampwirth, D. W. Capone, and J. M. Murduck, IEEE Trans. Magn. **25**, 2060 (1989).
[6] D. H. Kim, K. E. Gray, R. T. Kampwirth, K. C. Woo, D. M. McKay, and J. Stein, Phys. Rev. B **41**, 11642 (1990).
[7] Jyh-Haur Tyan and Juh Tzeng Lue, J. Appl. Phys. **75**, 325 (1994).
[8] A. Shoji, S. Kityu, and S. Kohjiro, Appl. Phys. Lett. **60**, 1624 (1992).
[9] Zhen Wang, Akira Kawakami, Yoshinori Uzawa, and Bokuji Komiyamaa, J. Appl. Phys. **79**, 7837 (1996).
[10] Zhen Wang, Hirotaka Terai, Akira Kawakami, and Yoshinori Uzawa, Appl. Phys. Lett. **75**, 701 (1999).
[11] Randolph E. Treece, Mike S. Osofsky, Earl F. Skelton, Syed B. Qadri, James S. Horwitz, and Douglas B. Chrisey, Phys. Rev. B **51**, 9356 (1995).
[12] L. Kang, P. H. Wu, J. R. Sh, W. X. Cai, S. Z. Yang, Z. M. Ji, and Z. Wang, Supercond. Sci. Technol. **16**, 1417 (2003).
[13] G. Lamura, J.-C. Villeger, A. Gauzzi, J. Le Cochec, J.-Y. Laval, B. Placais, N. Hadacek, and J. Bok, Phys. Rev. B **65**, 104507 (2002).
[14] John Q. Xiao and C. L. Chien, Phys. Rev. Lett. **76**, 1727 (1996).
[15] C. Stampfl and A. J. Freeman, Phys. Rev. B **71**, 024111 (2005).
[16] E. S. Sadki, Z. H. Barber, S. J. Lloyd, M. G. Blamire, and A. M. Campbell, Phys. Rev. Lett. **85**, 4168 (2000).
[17] Tsutomo Yamashita, Shogo Kitahara, Yutaka Onodera, Yukihiro Goto, and Tadao Aso, J. Appl. Phys. **43**, 4749 (1972).
[18] B. J. Feenstra, F. C. Klaassen, D. van der Marel, Z. H. Barber, R. Perez Pinaya, and M. Decroux, Physica C **278**, 213 (1997).
[19] Serdar Ogut and Karin M. Rabe, Phys. Rev. B **52**, R8585 (1995).
[20] E. C. Ethridge, S. C. Erwin, and W. E. Pickett, Phys. Rev. B **52**, R8589 (1995).
[21] K. Senapati, S. Chakrabarty, Leena K. Sahoo, and R. C. Budhani, Rev. Sci. Instrum. **75**, 141 (2004).
[22] J. Gilchrist and M. Konczykowski, Physica C **212**, 43 (1993).
[23] B. D. Cullity, *Elements of X-ray Diffraction* (Addison-Wesley, New York 1956).
[24] *Pulsed Laser Deposition of Thin Films*, edited by Douglas B. Chrisey and Graham K. Hubler (Wiley, New York, 1994).
[25] J. H. Mooij, Phys. Status Solidi A **17**, 521 (1973).
[26] Ali Yazdani and Aharon Kapitulnik, Phys. Rev. Lett. **74**, 3037 (1995).
[27] B. W. Dodson, W. L. McMillan, J. M. Mochel, and R. C. Dynes, Phys. Rev. Lett. **46**, 46 (1981).
[28] P. A. Lee and T. V. Ramakrishnan, Rev. Mod. Phys. **57**, 287 (1985).
[29] G. Reiss, J. Vancea, and H. Hoffmann, Phys. Rev. Lett. **56**, 2100 (1986).
[30] A. Nigro, G. Nobile, M. G. Rubino, and R. Vaglio, Phys. Rev. B **37**, 3970 (1988).
[31] D. Karecki, R. E. Pena, and S. Perkowitz, Phys. Rev. B **25**, 1565

(1982).
[32] J. M. Ziman, *Principles of the Theory of Solids* (Cambridge University Press, Cambridge, 1965), pp. 191.
[33] R. W. Simon, B. J. Dalrymple, D. Van Vechten, W. W. Fuller, and S. A. Wolf, Phys. Rev. B **36**, 1962 (1987).
[34] J. R. Clem, B. Bumble, S. I. Raider, W. J. Gallagher, and Y. C. Shih, Phys. Rev. B **35**, 6637 (1987).
[35] Y. Liu, D. B. Haviland, B. Nease, and A. M. Goldman, Phys. Rev. B **47**, 5931 (1993).
[36] Y. Imry and M. Strongin, Phys. Rev. B **24**, 6353 (1981).
[37] J. R. Clem and A. Sanchez, Phys. Rev. B **50**, 9355 (1994).
[38] *Magnetic Susceptibility of Superconductors and other Spin Systems*, edited by R. A. Hein, T. L. Francavilla, and D. H. Liebenberg (Plenum, New York 1991).
[39] W. Widder, L. Bauernfeind, H. F. Braun, H. Burkhardt, D. Rainer, M. Bauer, and H. Kinder, Phys. Rev. B **55**, 1254 (1997).
[40] K. H. Muller, Physica C **159**, 717 (1989).
[41] J. L. Cardoso and P. Pereyra, Phys. Rev. B **61**, 6360 (2000).
[42] V. Ambegaokar and A. Baratoff, Phys. Rev. Lett. **10**, 486 (1963).
[43] A. M. Campbell and J. E. Evetts, Adv. Phys. **21**, 199 (1972).
[44] C. J. van der Beek, M. Konczykowski, V. M. Vinokur, G. W. Crabtree, T. W. Li, and P. H. Kes, Phys. Rev. B **51**, 15492 (1995).
[45] Y. Yeshuran and A. P. Malozemoff, Phys. Rev. Lett. **60**, 2202 (1988).
[46] M. Suenaga, A. K. Ghosh, Y. Xu, and D. O. Welch, Phys. Rev. Lett. **66**, 1777 (1991).
[47] M. F. Schmidt, N. E. Israeloff, and A. M. Goldman, Phys. Rev. B **48**, 3404 (1993).
[48] D. N. Zheng, N. J. C. Ingle, and A. M. Campbell, Phys. Rev. B **61**, 15429 (2000).
[49] T. P. Orlando, E. J. McNiff, Jr., S. Foner, and M. R. Beasley, Phys. Rev. B **19**, 4545 (1979).
[50] L. D. Cooley, Y. F. Hu, and A. R. Moodenbough, Appl. Phys. Lett. **88**, 142506 (2006).